Anisotropic Scattering Caused by Apical Oxygen Vacancies in Thin Films of Overdoped High-Temperature Cuprate Superconductors

Da Wang[*], Jun-Qi Xu, Hai-Jun Zhang, and Qiang-Hua Wang[†]

National Laboratory of Solid State Microstructures & School of Physics, Nanjing University, Nanjing 210093, China
and Collaborative Innovation Center of Advanced Microstructures, Nanjing University, Nanjing 210093, China

There is a hot debate on the anomalous behavior of superfluid density ρ_s in overdoped La$_{2-x}$Sr$_x$CuO$_4$ films in recent years. The linear drop of ρ_s at low temperatures implies the superconductors are clean, but the linear scaling between ρ_s (in the zero temperature limit) and the transition temperature T_c is a hallmark of the dirty limit in the Bardeen-Cooper-Schrieffer (BCS) framework [I. Bozovic *et al.*, Nature (London) **536**, 309 (2016)]. This dichotomy motivated exotic theories beyond the standard BCS theory. We show, however, that such a dichotomy can be reconciled naturally by the role of increasing anisotropic scattering caused by the apical oxygen vacancies. Furthermore, the anisotropic scattering also explains the "missing" Drude weight upon doping in the optical conductivity, as reported in the THz experiment [F. Mahmood *et al.*, Phys. Rev. Lett. **122**, 027003 (2019)]. Therefore, the overdoped cuprates can actually be described consistently by the d-wave BCS theory with the unique anisotropic scattering.

Introduction.—For a long time, overdoped cuprate superconductors were believed to be described quite well by the Bardeen-Cooper-Schrieffer (BCS) theory [1,2]. However, in 2016, such a belief was challenged by the measurement of the superfluid density ρ_s using the mutual inductance technique on a large amount of high quality overdoped La$_{2-x}$Sr$_x$CuO$_4$ (LSCO) films [3]. Two seemingly contradicting results were reported: $\rho_s(0) - \rho_s(T) \propto T$ and $\rho_s(0) \propto T_c$ where $\rho_s(0)$ is the zero temperature value of $\rho_s(T)$ and T_c is the transition temperature. Within the conventional BCS theory, the former scaling law indicates the d-wave superconductors are very clean, but the latter is a result of dirty BCS superconductors [4]. This dichotomy regarding the dirtiness or cleanness of the overdoped cuprates motivated exotic theoretical investigations [5–12].

The superfluid density has also been measured by THz optical conductivity experiment [13], and is quantitatively consistent with the mutual inductance measurement [3]. In the meantime, the Drude fitting of the optical conductivity $\sigma_1(\nu)$ indicates the dirty limit [14,15]. So the same dichotomy also exists in optical measurements. Moreover, as yet another puzzle, $\sigma_1(\nu \to 0)$ should be identical to, but is fitted to be significantly smaller than the dc conductivity σ_{dc} [13]. This superficial loss of Drude weight seems to increase with overdoping.

In this Letter, we propose a scenario to resolve all of the above mysteries. We realize that in addition to the conventional isotropic scattering rate Γ_s [14,15], the apical oxygen vacancies cause an anisotropic scattering rate $\Gamma_d \cos^2(2\theta)$, with θ the azimuthal angle of the quasiparticle momentum relative to the antinodal direction. Since the low-energy nodal quasiparticles are barely affected by Γ_d, they reduce

the superfluid density linearly in temperature if in addition $\Gamma_s \to 0$. But the total scattering rate $\Gamma_\theta = \Gamma_s + \Gamma_d \cos^2(2\theta)$ determines the typical behavior $\rho_s(0) \propto T_c$ in the dirty limit. Meanwhile, the strong anisotropy in Γ_θ causes a continuous distribution of Lorentzian components in $\sigma(\nu)$, so that $\sigma_1(\nu \to 0)$ would be underestimated by extrapolation from finite frequencies if a single isotropic scattering rate were assumed instead [13].

Oxygen vacancies and the "cold spot" model.—From both early [16,17] and recent [18] studies, apical oxygen vacancies were found to be an important factor to prevent obtaining (high-quality) overdoped LSCO samples. Therefore, the effect of apical oxygen vacancies deserves study in overdoped cuprates carefully. This is another motivation of the present work.

In Fig. 1, we plot a configuration of one apical oxygen atom above the CuO$_2$ plane (only Cu sites plotted). Notice that since the carriers have $d_{x^2-y^2}$-like orbital content [19],
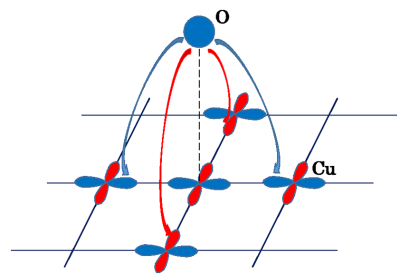

FIG. 1. Illustration of apical oxygen coupling to (effective) $d_{x^2-y^2}$ orbitals in the CuO$_2$ plane. Hoppings with opposite signs are labeled by blue and red colors, respectively.

there is no coupling between the oxygen and the $d_{x^2-y^2}$ orbital just below it. Therefore, the leading couplings are with the next nearest neighboring sites, giving the hopping integrals switching signs alternatively, as shown in Fig. 1. First, if there is no oxygen vacancy, the second order process of these out-of-plane hoppings gives an additional band dispersion $-4\kappa(\cos k_x - \cos k_y)^2$ where $\kappa = t_o^2/\varepsilon_o$ with t_o and ε_o the hopping amplitude and energy level distance between the apical oxygen and $d_{x^2-y^2}$ orbitals [20]. Such a dispersion has already enters the carrier band. Next, we consider one oxygen vacancy at the origin. Relative to the uniform background, the vacancy now leads to an additional term $H_i = \sum_{\delta\delta'\sigma} \kappa f_\delta f_{\delta'} c_{\delta\sigma}^\dagger c_{\delta'\sigma}$ where $f_\delta = 1(-1)$ for $\delta = \pm\hat{x}(\pm\hat{y})$ and σ denotes spin, which gives rise to the following scattering Hamiltonian:

$$H_i = \sum_{kk'\sigma} \frac{4\kappa}{N}(\cos k_x - \cos k_y)(\cos k'_x - \cos k'_y)c_{k\sigma}^\dagger c_{k'\sigma}, \quad (1)$$

where k and k' are momentums, and N is the number of copper atoms. Since the oxygen vacancies are out of plane and only couple to next nearest neighboring $d_{x^2-y^2}$ orbitals, the scattering strength is anticipated to be small. Under the Born approximation [4], H_i gives a scattering rate $\Gamma(k_x, k_y) \propto \Gamma_d(\cos k_x - \cos k_y)^2/4$. For analytical convenience but without loss of qualitative physics, throughout this work, we further assume a circular fermi surface and use wide band approximation, so that the scattering rate is only angle dependent, i.e.,

$$\Gamma_\theta = \Gamma_s + \Gamma_d\cos^2(2\theta) \quad (2)$$

where we have added the isotropic scattering rate Γ_s arising from, e.g., in-plane impurities. In the following calculations, Γ_s and Γ_d are our model parameters. In fact, this kind of scattering rate has been proposed to explain the transport phenomena in underdoped cuprates, called the "cold spot" model [21], where the Γ_d term is attributed to the pair fluctuations or interaction effects, which hence is expected to decrease upon doing. But here, in our case, the Γ_d term is caused by oxygen vacancies and should increase upon doping, according to both early [16,17] and recent [18] experiments.

We now look at the effect of the anisotropic scattering Γ_d on single particle excitations. By choosing the d-wave pairing function $\Delta(\theta) = \Delta_0 \cos(2\theta)$ and fixing $\Gamma_{s,d} = 0.2\Delta_0$, we calculate the density of states (DOS) $\rho(\omega) = \int(d\theta/2\pi)\rho(\omega, \theta)$, where $\rho(\omega, \theta)$ is the partial DOS (PDOS) given by

$$\rho(\omega, \theta) = \frac{\mathcal{N}}{\pi}\int d\varepsilon \left[\frac{\Gamma_\theta}{(\omega - E_\theta)^2 + \Gamma_\theta^2} + \frac{\Gamma_\theta}{(\omega + E_\theta)^2 + \Gamma_\theta^2}\right] \quad (3)$$

where $\mathcal{N}$ is the normal state DOS and $E_\theta = \sqrt{\varepsilon^2 + \Delta(\theta)^2}$. $\rho(\omega)$ and $\rho(\omega, \theta)$ are plotted in Figs. 2(a)–2(d). In the calculations, we perform the integrals over ε and θ using the standard numerical integral technique. Figure 2(a) is the typical behavior of the conventional d-wave superconductor with the isotropic scattering rate: the zero energy cusp and coherence peak are both smeared out by the isotropic scattering rate. Differently, the Γ_d scattering shown in Fig. 2(b) only suppresses the coherence peak but does not change the zero energy cusp, as a result of the vanishing of the scattering rate for nodal quasiparticles. Accordingly, we can divide the energy space into two regions: a lower energy "clean" one and a higher energy "dirty" one. The above picture is also seen clearly from the PDOS in Fig. 2(d), where the spectral becomes smeared out for high energy quasiparticles (near the antinodes) but remains sharp for low energy ones (near the nodes).
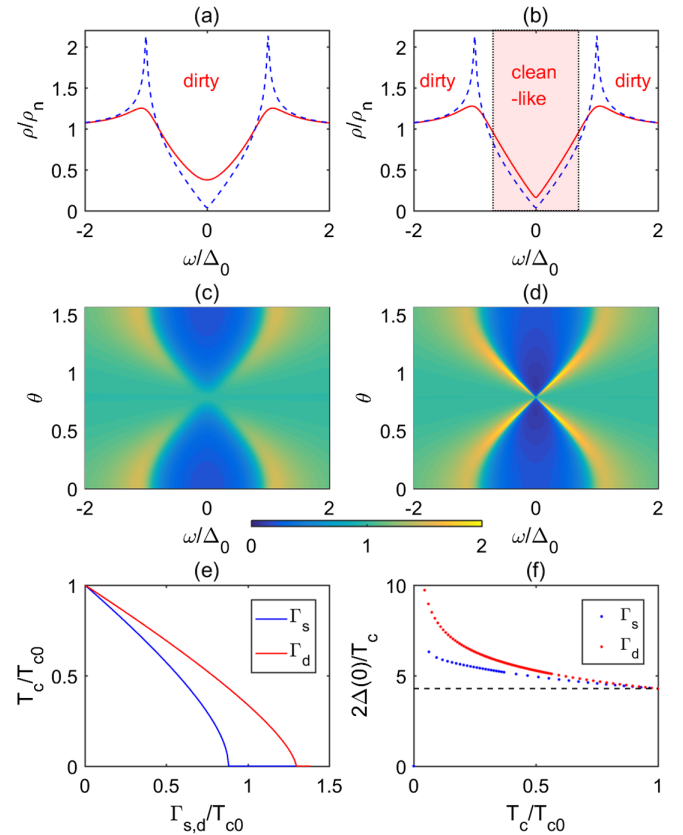

FIG. 2. (a) The DOS ρ versus ω in the case of pure isotropic scattering $\Gamma_s = 0.2\Delta_0$ (solid line). For comparison, the dashed line shows the DOS in the clean limit. (b) The same as (a) but in the case of pure anisotropic scattering $\Gamma_d = 0.2\Delta_0$. The shaded region highlights the similarity to the clean limit. (c) and (d) are angle-dependent PDOS in the presence of scattering corresponding to (a) and (b), respectively. (e) T_c/T_{c0} versus Γ_s/T_{c0} (blue) and Γ_d/T_{c0} (red) for the two types of scatterings. (f) The ratio $2\Delta_0(0)/T_c$ versus T_c/T_{c0} (red and blue dots) for the two cases considered in (e), in comparison to the clean limit result (dashed line).

The dirty BCS theory for d-wave superconductors [22] is a direct generalization of the Abrikosov-Gor'kov (AG) theory [23], since the potential scattering here causes pair breaking which is similar to the magnetic impurities in s-wave superconductors. The gap Δ_0 is determined by the self-consistent equation

$$1 = \lambda T \sum_{\omega_n > 0} \int d\theta \frac{\phi_\theta^2}{\sqrt{\omega_n^2 + 2|\omega_n|\Gamma_\theta + \Gamma_\theta^2 + \Delta_0^2 \phi_\theta^2}} \quad (4)$$

where λ is the BCS coupling constant, $\omega_n = (2n-1)\pi T$ the Matsubara frequency, and $\phi_\theta = \cos 2\theta$ the d-wave form factor [24]. In numerical calculations, we use $\lambda = 0.3$ and $\Omega = 800$, which gives $T_{c0} = 1.134\Omega e^{-2/\lambda} = 1.15$ for clean superconductors (with this setup, $0.87T_{c0}$ is taken as the energy unit). By letting $\Delta_0 \to 0$, we obtain the generalized T_c formula

$$\ln \frac{T_{c0}}{T_c} = \frac{1}{\pi} \int d\theta \phi_\theta^2 \left[\psi\left(\frac{1}{2} + \frac{\Gamma_\theta}{2\pi T_c}\right) - \psi\left(\frac{1}{2}\right) \right] \quad (5)$$

where $\psi(z)$ is the digamma function. The results of T_c vs Γ_s and Γ_d are shown in Fig. 2(e). A stronger Γ_d is needed to kill superconductivity as the low energy excitations are less affected. In Fig. 2(f), we show the results of $2\Delta_0/T_c$. It is interesting to find that the anisotropic scattering drives the ratio farther away from the BCS prediction 4.28 in the clean limit to values as large as ∼10. In the literature, a large gap-T_c ratio is often taken as an indication of strong coupling superconductivity. Here, the anisotropic scattering gives another interpretation.

Superfluid density.—After recognizing the clean-dirty dichotomy caused by oxygen vacancies at the single particle level, we turn to discuss the superfluid density, which can be obtained as [25]

$$\rho_s = e^2 \mathcal{N} v_F^2 T \sum_{\omega_n} \int d\theta \frac{\Delta_\theta^2 \cos^2\theta}{(\omega_n^2 + 2|\omega_n|\Gamma_\theta + \Gamma_\theta^2 + \Delta_\theta^2)^{3/2}} \quad (6)$$

where v_F is the Fermi velocity. Here, the current vertex correction can be proven to vanish in the noncrossing approximation as a result of the factorized scattering potential [Eq. (1)], as shown in the Supplemental Material [26]. In Figs. 3(a) and 3(b), ρ_s vs T is plotted for pure Γ_s and Γ_d scatterings, respectively. The most obvious difference is that any nonzero Γ_s causes power law temperature dependence of $\rho_s(T)$, but Γ_d preserves the linear dependence as in the clean limit. This is already anticipated from the DOS feature in Fig. 2(b) because the normal fluid density ρ_n is roughly determined by quasiparticles and thus satisfies $\rho_n(T) - \rho_n(0) \propto T$, leaving the superfluid density satisfying $\rho_s(0) - \rho_s(T) = \rho_n(T) - \rho_n(0) \propto T$.
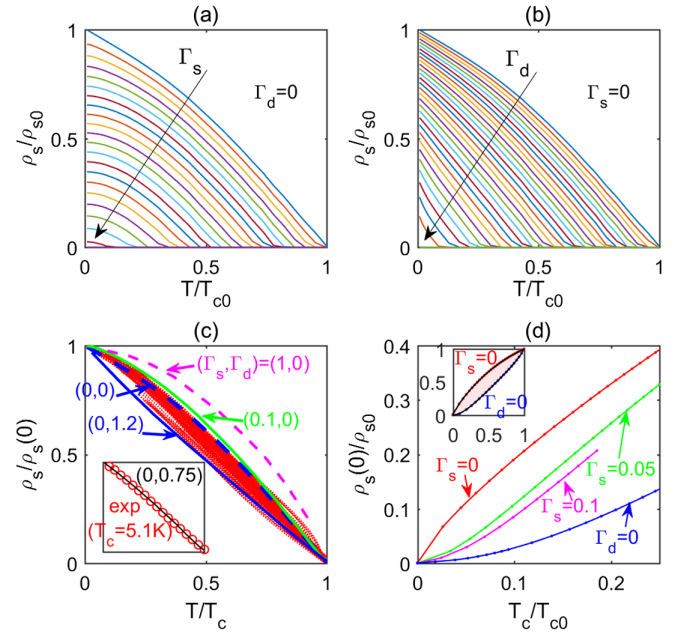

FIG. 3. (a) Superfluid density ρ_s/ρ_{s0} as a function of T/T_{c0} in the case of isotropic scattering ($\Gamma_d = 0$), for various values of Γ_s which increases uniformly from top to bottom. Here $\rho_{s0} = \rho_s(0)$ in the clean limit. (b) The same as (a) but in the case of anisotropic scattering ($\Gamma_s = 0$) and for various values of Γ_d. (c) $\rho_s/\rho_s(0)$ as a function of T/T_c for $(\Gamma_s, \Gamma_d) = (0,0)$ (dashed blue), (0.1,0) (green), (1,0) (dashed pink), (0,1.2) (blue). The red dots show all 100 groups of experimental data [3] for comparison. The inset shows the fit to the experimental data with $T_c = 5.1$ K using $(\Gamma_s, \Gamma_d) = (0, 0.75)$. (d) $\rho_s(0)/\rho_{s0}$ as a function of T_c/T_{c0}. The lines are obtained by fixing one of (Γ_s, Γ_d) (as indicated) while varying the other. The inset shows two similar curves by fixing $\Gamma_s = 0$ and $\Gamma_d = 0$, respectively, in a broader scale. The results of all other cases (not shown) fall within the shaded regime bounded by these two curves. In (c) and (d), the insets share the same axis labels as for the main panels.

In real materials, both Γ_s and Γ_d are expected to coexist. In order to make quantitative comparisons with the experiment, we renormalize T and ρ_s by T_c and $\rho_s(0)$, respectively, as shown in Fig. 3(c). We have superposed the experimental data of all 100 samples with T_c ranging from 41.6 to 5.1 K [3], shown as the red dots. Four typical theoretical curves are plotted: $(\Gamma_s, \Gamma_d) = (0, 0)$, (0.1,0), (1,0), and (0,1.2). As can be seen, almost all the experimental data reside within the region enclosed by the curves of (0.1,0) (green line) and (0,1.2) (blue line); while if Γ_s is large and dominant, as the (1,0) line shows, the renormalized $\rho_s - T$ curve bends more significantly, which is at odds with the experimental data. These observations indicate the more important role of Γ_d. As an example, the experimental data (open circles) with $T_c = 5.1$ K are shown in the inset, which is clearly very linear. We can fit the data with pure $\Gamma_d = 0.75$ (line) quite well.

Another key observation of the experiment [3] is the linear relationship between $\rho_s(0)$ vs T_c. To see that, we plot

our results in Fig. 3(d). Pure Γ_s and Γ_d scatterings correspond to blue and red curves, which enclose the physical region (shaded region in the inset), in which $\rho_s(0)$ is always roughly proportional to T_c although not exactly. Therefore, this is a hallmark of the dirty BCS superconductors regardless of isotropic (Γ_s) or anisotropic (Γ_d) scatterings. Furthermore, we have also fix $\Gamma_s = 0.05$ and 0.1 and tune Γ_d to suppress T_c. Both of them show the bending behavior near $T_c \to 0$, showing much better behavior than the separate scattering cases in view of the experimental data.

Optical conductivity.—From the Kubo formula, the optical conductivity $\sigma_1(\nu)$ can be obtained as [29]

$$\sigma_1(\nu) = \frac{\mathcal{N}e^2 v_F^2}{2\pi^3} \int d\varepsilon d\theta d\omega \frac{f(\omega) - f(\omega + \nu)}{\nu} \cos^2\theta$$
$$\times \mathrm{tr}[\mathrm{Im}G(\omega, \varepsilon, \theta)\mathrm{Im}G(\omega + \nu, \varepsilon, \theta)] \quad (7)$$

where $f(\omega)$ is the Fermi distribution function, $G(\omega, \varepsilon, \theta)$ is the Green's function in the Nambu space: $G^{-1} = (\omega + i\Gamma_\theta)\sigma_0 - \varepsilon\sigma_3 - \Delta_0\phi_\theta\sigma_1$ with $\sigma_{0,1,3}$ the identity and Pauli matrices. By numerical calculations, we obtain the frequency dependence of $\sigma_1(\nu)$ in both normal and superconducting states (with $\Delta_0 = 1$ as the energy unit), as shown in Figs. 4(a) and 4(b), respectively. In the normal state, as Γ_d increases, $\sigma_1(\nu)$ becomes more and more broadened to show long tail behavior. This is an important feature obtained in the cold spot model [21]. In the superconducting state, a nonzero Γ_d breaks the universal conductivity [30], which applies only in the case of pure Γ_s scattering as shown in the inset of Fig. 4(b). Furthermore, we renormalize the superconducting state $\sigma_1(\nu)$ by the normal state value $\sigma_{1n}(\nu)$ to obtain the results shown in Fig. 4(c). The resulted curves show similar behavior to the DOS at low frequencies: nearly linear ν dependence if Γ_d dominates, which is quite different from the case of pure Γ_s scattering (inset) with quadratic ν dependence. This can be used to examine the types of scattering in future experiments.

The most obvious feature when Γ_d dominates is the behavior of $\sigma_1(\nu)$ is no longer a simple Lorentian-like Drude peak (as in the case of isotropic scattering), since the quasiparticles experience angle dependent scattering rates. In fact, the conductivity should be an integration over a continuous distribution of Lorentzian components. Since the Lorentzian is sharper and higher for smaller scattering rates, the overall line shape of $\sigma_1(\nu)$ should be steeper as the frequency approaches zero. Therefore, if the finite frequency data are used to perform the fit to a single Lorentzian-like Drude peak, as in the THz experiment, the extrapolated value of $\sigma_1(\nu \to 0)$ will be lower than the actual one, leading to superficial "missing" of the Drude weight. As an example, in Fig. 4(d) we fit the experimental data with $T_c = 17.5$ K (symbols) in both normal (blue) and superconducting (red) states [13]. The best fits with only Γ_s
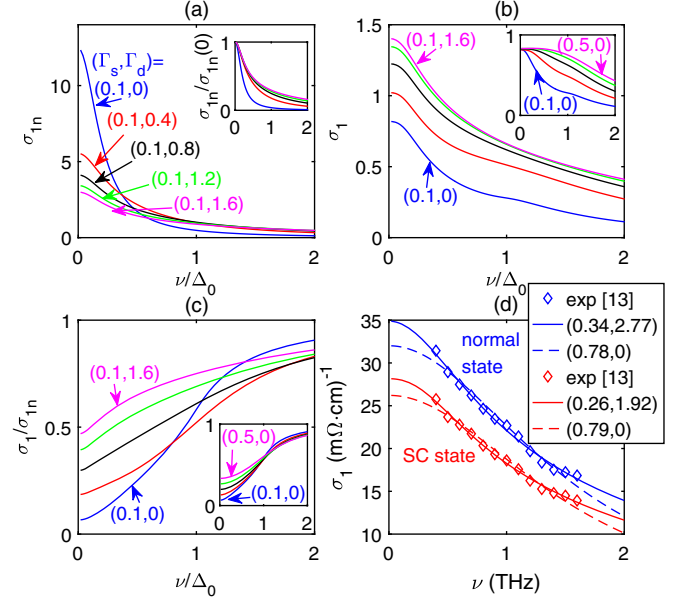

FIG. 4. (a) Optical conductivity σ_{1n} versus frequency ν in the normal state for various cases of (Γ_s, Γ_d) (as indicated) in unit of Δ_0. The inset is a replot of σ_1 in the main panel but normalized by $\sigma_{1n}(0)$. (b) The same as (a) but for the superconducting state conductivity σ_1. The inset shows the result for isotropic scattering, revealing the universal conductivity in the zero frequency limit. (c) σ_1/σ_{1n} versus ν, with σ_{1n} and σ_1 from (a) and (b), respectively. The inset is for isotropic scattering. In (a)–(c), the line color is associated with the scattering parameter setting identically, and in (b) and (c), the insets share the same axis labels as for the main panels. (d) Best fits (lines) to the experimental data (symbols) with $T_c = 17.5$ K measured at 22 K (blue) and 1.6 K (red) [13]. The dashed lines are best fits with Γ_s alone, and the solid lines include both Γ_s and Γ_d.

(dashed lines) are found to underestimate $\sigma_1(\nu \to 0)$ and the spectral weight, as compared to the result with both Γ_s and Γ_d (solid lines). Since the pairing gap Δ_0 is not available in the experiment, we take it also as a parameter, and the fitted value is 1.11 THz. More systematic fitting for a series of overdoped samples can be found in the Supplemental Material [26], which supports our main point that apical oxygen vacancy increases with overdoping, leading to larger Γ_d scattering.

Summary and discussions.—In summary, we have found that the apical oxygen vacancies give rise to an anisotropic scattering rate $\Gamma_d \cos^2(2\theta)$ which causes a clean-dirty dichotomy for low-high energy excitations. This provides a natural explanation of the anomalous behavior of the superfluid density and THz optical conductivity in the experiments. Therefore, we conclude that the superconducting states of overdoped cuprates are still captured by the BCS theory, as long as the anisotropic scattering rate is adequately considered.

Finally, we make some remarks. (1) In this work, we have omitted many material-dependent details (such as specific tight-binding models, pairing interactions and

interaction effects) in order to obtain universal results. The doping dependence enters the problem via the scattering rate Γ_d, which increases with doping. (2) The anisotropic scattering rate has been reported in angle-dependent magnetoresistivity experiments in Nd-LSCO [31] and $Tl_2Ba_2CuO_{6+\delta}$ [32]. But to the best of our knowledge, there has not been such report in overdoped LSCO films. A systematic study of the anisotropic scattering rate can check our model and finally answer the question on whether overdoped cuprates are dirty BCS superconductors or not. (3) Our prediction suggests that it is necessary to extend the optical measurements down to even lower frequency (e.g., GHz) in order to obtain accurate behavior of the optical conductivity. (4) About superfluid density, there are two other kinds of scalings reported in literature: Uemura's law [33] $\rho_s(0) \propto T_c$ and Homes' law $\rho_s(0) \propto \sigma_{dc} T_c$ [34]. The former is obtained in underdoped cuprates, where phase fluctuations are very strong and cannot be neglected. [35]. On the other hand, Homes' law can be explained by dirty BCS superconductors with pair-preserving impurities only [4,36]. Here, in the overdoped LSCO films, the oxygen vacancies are pair breaking, hence Homes' law does not apply. (5) Recently, apical oxygen vacancies have also been observed in optimally doped $YBa_2Cu_3O_{7-x}$ [37]. Then, according to our study, $\sigma_1(\nu)$ at low frequency should be nonstandard Drude-like, which may be consistent with the early microwave experiment [38]. Furthermore, if the apical oxygen vacancies are widely present in different families of cuprates, then the effect of Γ_d scattering should be considered carefully in future studies.

---

*dawang@nju.edu.cn
†qhwang@nju.edu.cn

[1] P. A. Lee, N. Nagaosa, and X.-G. Wen, Rev. Mod. Phys. **78,** 17 (2006).

[2] B. Keimer, S. A. Kivelson, M. R. Norman, S. Uchida, and J. Zaanen, Nature (London) **518,** 179 (2015).

[3] I. Božović, X. He, J. Wu, and A. T. Bollinger, Nature (London) **536,** 309 (2016).

[4] A. A. Abrikosov, L. Gorkov, and I. E. Dzialoshinskii, *Methods of Quantum Field Theory in Statistical Physics* (Prentice-Hall, NJ, 1963).

[5] I. Božović, J. Wu, X. He, and A. Bollinger, Physica (Amsterdam) **558C,** 30 (2019).

[6] J. Zaanen, Nature (London) **536,** 282 (2016).

[7] F. Herman and R. Hlubina, Phys. Rev. B **97,** 014517 (2018).

[8] W. Fu, Y. Gu, S. Sachdev, and G. Tarnopolsky, Phys. Rev. B **98,** 075150 (2018).

[9] D. Wang, Chin. Phys. B **27,** 057401 (2018).

[10] B. Goutéraux and E. Mefford, Phys. Rev. Lett. **124,** 161604 (2020).

[11] P. W. Phillips, L. Yeo, and E. W. Huang, Nat. Phys. **16,** 1175 (2020).

[12] Z.-X. Li, S. A. Kivelson, and D.-H. Lee, npj Quantum Mater. **6,** 36 (2021).

[13] F. Mahmood, X. He, I. Božović, and N. P. Armitage, Phys. Rev. Lett. **122,** 027003 (2019).

[14] N. R. Lee-Hone, J. S. Dodge, and D. M. Broun, Phys. Rev. B **96,** 024501 (2017).

[15] N. R. Lee-Hone, V. Mishra, D. M. Broun, and P. J. Hirschfeld, Phys. Rev. B **98,** 054506 (2018).

[16] J. B. Torrance, Y. Tokura, A. I. Nazzal, A. Bezinge, T. C. Huang, and S. S. P. Parkin, Phys. Rev. Lett. **61,** 1127 (1988).

[17] H. Sato, A. Tsukada, M. Naito, and A. Matsuda, Phys. Rev. B **61,** 12447 (2000).

[18] G. Kim, G. Christiani, G. Logvenov, S. Choi, H.-H. Kim, M. Minola, and B. Keimer, Phys. Rev. Mater. **1,** 054801 (2017).

[19] F. C. Zhang and T. M. Rice, Phys. Rev. B **37,** 3759 (1988).

[20] T. Xiang and J. M. Wheatley, Phys. Rev. Lett. **77,** 4632 (1996).

[21] L. B. Ioffe and A. J. Millis, Phys. Rev. B **58,** 11631 (1998).

[22] H. Alloul, J. Bobroff, M. Gabay, and P. J. Hirschfeld, Rev. Mod. Phys. **81,** 45 (2009).

[23] A. A. Abrikosov and L. P. Gor'kov, Sov. Phys. JETP **12,** 1243 (1961).

[24] Exactly speaking, the frequency summation should be bounded with a soft-cutoff (with the form of a boson propagator) instead of the hard cutoff used here. However, only the latter can be mapped to the momentum cutoff strategy as in the BCS treatment.

[25] P. Coleman, *Introduction to Many-Body Physics* (Cambridge University Press, Cambridge, England, 2015).

[26] See Supplemental Material at http://link.aps.org/supplemental/10.1103/PhysRevLett.128.137001 for calculation details and further discussions, which includes Refs. [3,4,13,18,23,25,27,28].

[27] K. P. Kramer *et al.*, Phys. Rev. B **99,** 224509 (2019).

[28] P. A. Lee and T. V. Ramakrishnan, Rev. Mod. Phys. **57,** 287 (1985).

[29] P. J. Hirschfeld, P. Wölfle, J. A. Sauls, D. Einzel, and W. O. Putikka, Phys. Rev. B **40,** 6695 (1989).

[30] P. A. Lee, Phys. Rev. Lett. **71,** 1887 (1993).

[31] G. Grissonnanche, Y. Fang, A. Legros, S. Verret, F. Laliberté, C. Collignon, J. Zhou, D. Graf, P. A. Goddard, L. Taillefer, and B. J. Ramshaw, Nature (London) **595,** 667 (2021).

[32] M. Abdel-Jawad, M. P. Kennett, L. Balicas, A. Carrington, A. P. Mackenzie, R. H. McKenzie, and N. E. Hussey, Nat. Phys. **2,** 821 (2006).

[33] Y. J. Uemura *et al.*, Phys. Rev. Lett. **62,** 2317 (1989).

[34] C. C. Homes, S. V. Dordevic, M. Strongin, D. A. Bonn, R. Liang, W. N. Hardy, S. Komiya, Y. Ando, G. Yu, N. Kaneko, X. Zhao, M. Greven, D. N. Basov, and T. Timusk, Nature (London) **430**, 539 (2004).

[35] V. J. Emery and S. A. Kivelson, Nature (London) **374**, 434 (1995).

[36] V. G. Kogan, Phys. Rev. B **87**, 220507(R) (2013).

[37] S. T. Hartman, B. Mundet, J.-C. Idrobo, X. Obradors, T. Puig, J. Gázquez, and R. Mishra, Phys. Rev. Mater. **3**, 114806 (2019).

[38] P. J. Turner, R. Harris, S. Kamal, M. E. Hayden, D. M. Broun, D. C. Morgan, A. Hosseini, P. Dosanjh, G. K. Mullins, J. S. Preston, R. Liang, D. A. Bonn, and W. N. Hardy, Phys. Rev. Lett. **90**, 237005 (2003).